THE JOURNAL OF PHYSICAL CHEMISTRY B

Article

pubs.acs.org/JPCB

Structural Photodynamic Behavior of Topotecan, a Potent Anticancer Drug, in Aqueous Solutions at Different pHs

Maria Rosaria di Nunzio, YiLun Wang, and Abderrazzak Douhal*

Departamento de Química Física, Facultad de Ciencias Ambientales y Bioquímica, and INAMOL, Universidad de Castilla-La Mancha, Avenida Carlos III, S/N, 45071 Toledo, Spain

Supporting Information

ABSTRACT: In this work, we report on photophysical studies of the anticancer drug topotecan (TPT) in aqueous solutions at different pHs. We used steady-state (UV−visible absorption and emission) and time-resolved picosecond (ps) emission spectroscopies to investigate the role of the H-bonding interactions as well as the proton concentration (pH = 0.48−7.40) on the behavior of topotecan (TPT) in its ground- (S_0) and electronically first (S_1) excited-states. At physiological conditions (pH = 7.40), the drug exists at S_0 in equilibrium between the enol (E), cation (C), and zwitterion (Z) forms. The photoformation of Z* (τ_Z = 5.83 ns) occurs from directly excited (λ_{exc} = 371 nm) E as the two-step reaction: E*→C*→Z*. In this process, a very fast (less than 10 ps) protonation of E* leads to C*, which subsequently undergoes fast (580 ps) deprotonation to give Z* as the final photoproduct. At higher proton concentrations (pH = 0.48−1.31), a ground-state equilibrium exists between three different cationic species (C1, C2, and C3). The proton motion from the acidic solution to the C forms of TPT to give the reactions C1*→C2*→C3* is governed by the proton diffusion. In these conditions, both dynamic and static quenching occurs. The rate constant values k^*_{DPT1} and k^*_{DPT2} for the direct protonation of C1* and C2*, respectively, depend on the pH of the surrounding. The number of protons implicated in the reaction changes from ∼2 (pH = 0.48−0.78) to ∼1 (pH = 0.78−1.31), thus indicating the existence of two different reactions and proton-transfer dynamics. These results evidence the conformational, structural, and dynamical changes of aqueous solutions of TPT with the pH of the environment. They should help to understand the molecular structure/activity of TPT at cellular level.

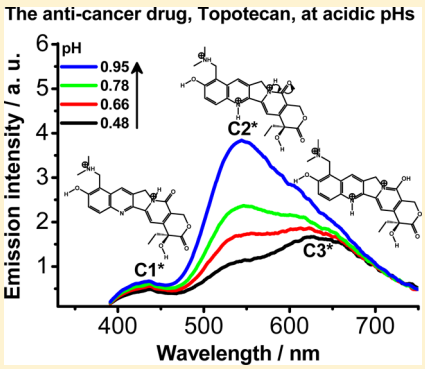

1. INTRODUCTION

Camptothecins (CPTs) have shown relevant therapeutic applications in medicine, belonging to a class of antitumoral agents.[1−3] The basic compound camptothecin (CPT) is a natural alkaloid extracted, for the first time, from the Chinese tree *Camptotheca acuminata*.[4] The biological target of CPT in clinical applications is the human topoisomerase I (Top1) enzyme, which is essential for the control of DNA supercoiling.[5−7] The key role of the drug consists of stabilizing the Top1−DNA biological complex, thus producing lethal DNA strand breaks. Both the nature and strength of the bindings (H-bonding and stacking interactions) between CPT and the flanking base pairs significantly influence the stability of the Top1−DNA complex.[8] Because of a high degree of toxicity observed in normal tissues for the drug in its original and natural form,[9] many efforts have been directed toward the synthesis of more soluble, hydrolytically more stable, and less toxic CPT-derivatives. In this respect, the drug topotecan (TPT) (9-[(dimethylamino)methyl]-10-hydroxy-camptothecin), in combination with other chemotherapy agents, is currently applied in ovarian,[10] small-cell lung,[11] and, more recently, cervical cancer[12] treatments. The basic structure of TPT consists of five rings out of which four (A, B, D, and E) are six-membered and one (C) is five-membered (Scheme 1). Two substituents, a dimethylaminomethylene and a hydroxyl group, are on the A-ring at the 9- and 10-positions, respectively.

Scheme 1. Molecular Structure of TPT in Its Closed-Ring Form[a]

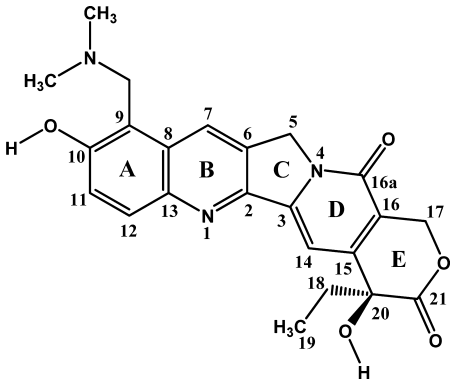

[a]The labeling of the C atoms is shown.

The presence of the 6-hydroxyquinoline (6HQ, A- and B-rings) subunit and the 9-dimethylaminomethylene group give to the molecule a multifunctional nature, making feasible the

Received: April 20, 2012
Revised: June 18, 2012
Published: June 19, 2012

instauration of different excited-state prototropic processes. On the other hand, quinoline derivatives are well-known to give birth to different excited-state structures, including triplet states.[13−16]

The photodynamic behavior of TPT in solution has been mainly investigated by the use of UV−visible absorption and fluorescence (stationary and time-resolved) spectroscopies.[17−23] The equilibria between the different forms of the drug were determined by the use of both spectroscopical[21] and theoretical (DFT)[24] methods at moderately acidic and physiological pH values. The emission spectrum of TPT is sensitive to solvent polarity.[22] In aqueous buffer solution, a unique fluorophore (τ = 5.9 ns) was observed upon excitation with either one or two photons. It was assigned to the zwitterionic (Z) form of the drug, as the result of an excited-state intramolecular proton-transfer (ESIPT) reaction involving the 9-dimethylaminomethylene and 10-hydroxyl groups.[22] However, among the variety of reports on TPT in solution, we found no additional information on the effect of proton concentration on its excited-state dynamics. An important effect of the pH of the medium and/or light exposure on the pharmacological activity of many promising anticancer, antiviral, and anti-inflammatory drugs has been recently reported.[25−29] The entire biological system [Top1−CPTs−DNA complex plus solvent] is large and flexible, and the drug is perturbed by several structural factors and chemistry-induced electronic rearrangements. Indeed, a spectroscopical and dynamical characterization of the different tautomeric forms of aqueous CPT and CPT modified drugs in diluted water solution is helpful for a better understanding of the mechanisms of interaction of CPTs within the ternary complex, which has not completely clarified. Recently, we have studied the behavior of TPT at its ground state and first electronically excited states in organic solvents of different nature (THF, DCM, ACN, and MeOH) and in aqueous solutions at pH = 6.24 and 12.15.[30] The obtained results showed, for all the studied solvents, the existence of a multiple emission due to an excited-state proton-transfer (ESPT) reaction that converts the initial absorbing species (cation, C, and/or enol, E) in the respective zwitterion (Z) and/or anion (A). The nature of the H-bonds that are formed between the drug and the solvent molecules largely affects the rate constant of the proton-transfer reaction.

This report provides and discusses a deeper investigation, using steady-state (UV−visible absorption and emission) and time-resolved picosecond (ps) emission studies, on the role of proton concentration on the spectroscopical and dynamical properties of aqueous solutions of TPT at different pHs (0.48−7.40). The existence of a multiple emission is observed at all the studied proton concentrations. The mechanism and, thus, the rate of the proton motion are strongly affected by the pH of the medium. The dynamics of the drug previously observed at near neutral pH (6.24)[30] is preserved at physiological conditions. Five different cationic species (C1, C2, C3, C4, and C5) are involved at pH < 7.40. Their relative contribution depends on the pH of the medium. Proton diffusion governs the dynamics under very acidic conditions (pH = 0.48−1.31). Here, a two-step protonation process involving three different cationic species (C1, C2, and C3) occurs at both the S_0 and S_1 states. The excited-state proton-transfer (ESPT) time constants determined for C1* (46 and 145 ps at pH = 0.48 and 1.31, respectively) and C2* (93 and 526 ps at pH = 0.48 and 1.31, respectively) largely depend on the proton concentration. The number of hydronium ions ($n \sim 1$), directly connected to the excited TPT, increases to ~2 in more acidic conditions (pH ≤ 0.78). These results clearly reflect the influence of the surrounding (pH and H-bonding ability) on the ground- and excited-state dynamics of TPT, thus providing new insights on the photobehavior of the drug in aqueous solution at physiological conditions (pH = 7.40) as well as in a wide range of proton concentration.

2. EXPERIMENTAL SECTION

(*S*)-(+)-Topotecan hydrochloride (TPT, ≥ 98%) was from Sigma-Aldrich. Deionized water, chloridric acid containing 33% HCl (Scharlau), and potassium mono(and di)hydrogen phosphate (Merck, > 99%) were used to prepare the aqueous solutions of different pHs. The relative error of the measured pH was estimated to be around 2%. Steady-state absorption and emission spectra were recorded on Varian (Cary E1) and Perkin-Elmer LS 50B spectrophotometers, respectively. Emission lifetimes were measured by using a picosecond time-correlated single-photon-counting (TCSPC) spectrophotometer (FluoTime 200, PicoQuant) described elsewhere.[31] The sample was excited by a 40 ps pulsed (20 MHz) laser centered at 371 or 433 nm. The instrumental response function (IRF) of the apparatus was typically 65 ps. The fluorescence signal, gated at the magic angle (54.7°), was monitored at a 90° angle to the excitation beam at discrete emission wavelengths using a 100 mm monochromator between the sample and the Hamamatsu microchannel plate photomultiplier (R3809-U21). Decay data were analyzed using the FluoFit software package (PicoQuant). Exponential decay functions were convoluted with the experimental response function and fit to the experimental decay. The quality of the fits was characterized in terms of the reduced χ^2 value and the distribution of residuals. All the measurements were done at 293 K.

3. RESULTS AND DISCUSSION

3.1. Steady-State Observation. *UV−Visible Absorption Spectra.* The influence of the proton concentration on the properties of TPT in its ground state and electronically first excited states was investigated in a wide range of pH values (0.48−7.40). Figure 1A shows the normalized UV−visible absorption spectra at selected pHs (0.78 and 7.40), while Figure 1B illustrates the changes under more acidic conditions (pH = 0.48−3.35). TPT has been already reported to undergo several equilibria between different structures depending on the pH of the solution.[21] In particular, four pK_a values have been experimentally determined: pK_{a1} < 0.8 and pK_{a2} ~ 3.6, assigned to the protonation of N1 and N4 atoms, respectively, and pK_{a3} = 6.5 and pK_{a4} = 10.7, relative to the deprotonation of the 10-hydroxyl and the 9-dimethylaminomethylene group, respectively (Supporting Information, Table 1S).[21] The experimental finding and related assignments have been also corroborated using theoretical methods (AM1, INDO/S, and DFT).[21,24a] Very recently, the coexistence of analogous prototropic equilibria in the several CPT derivatives has been investigated both theoretically (quantum chemical calculations) and experimentally (UV−visible and circular dichroism spectroscopy).[24b] In particular, high values of protonation ability have been computed (through DFT methods) for the electron-rich centers (the nitrogen atoms) of the drugs, and the wavelengths of the UV−visible absorption intensity maxima of the mono-, di-, and triprotonated forms have been determined.

On the basis of the above pK_a values, and depending on the pH of the medium, we propose the following structures of TPT. Table 2S in Supporting Information shows the steady-state UV−visible absorption and fluorescence data of most of them, and a

dx.doi.org/10.1021/jp303826c | J. Phys. Chem. B 2012, 116, 8182−8190

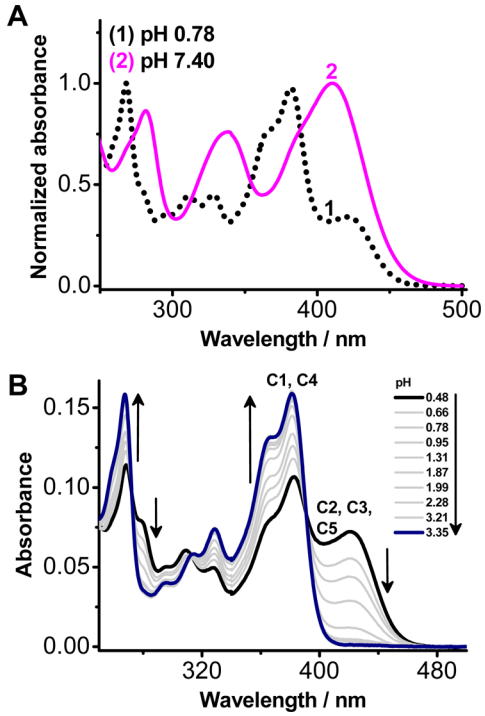

Figure 1. (A) Normalized absorption spectra of TPT in acidic water (pH = 0.78) (1) and in phosphate buffer solution (pH = 7.40) (2). (B) UV−visible absorption spectra of TPT in aqueous solutions as a function of pH. The $S_0 \rightarrow S_1$ absorption bands of the cationic species are marked as C1, C2, C3, C4, and C5.

comparison with the literature data is also given to sustain our assignments.

pH = 0.48−1.31. At these high proton concentrations, the drug exists principally in three ionic structures (Scheme 2). The first one, having the absorption maximum at 381 nm, is assigned to a dication (C1) species, which has protonation on both the 9-dimethylaminomethylene group and the N4 atom. The additional protonation of the N1 atom leads to the appearance of the second species, C2, characterized by a total charge of +3 on its molecular frame and it absorbs in the long-wavelength region (λ_{abs}^{max} = 421 nm, Figure 1A, pH = 0.78).[21] Protonation of the quinoline moiety has been previously observed for CPT (pK_a = 1.14) and 10-CPT (pK_a = 1.8), resulting in the appearance of quinolinium-type red-shifted absorption ($\Delta\lambda$ = 35−40 nm) band.[26,32] It has been shown by both experimental and theoretical data that the TPT structure with a proton on the oxygen atom at C16a rather than on N4 atom is the most stable one.[21] Such protonation leads to the transformation of the keto group at C16a into hydroxyl group, thus creating the third species C3 (Scheme 2). In the latter one, the formation of a double bond between the N4 and C16a atoms generates a complete aromatization of the D-ring, thus accounting for a larger stabilization.[21] The quinolinium-type structures of the cations, C2 and C3, display the maximum absorption intensity as the pH decreases to 0.48, while C1 is the predominant species at pH = 1.31. Three isosbestic points, at 390, 314, and 272 nm, are clearly observed in the absorption spectra shown in Figure 1B.

pH = 1.31−3.35. At this pHs range, and based on the pK_a value of N4 (∼3.6),[21] we have to take into account additional dicationic species, C4 and C5 (Supporting Information, Scheme 1S), coming from N4-deprotonated species C1 and C2, respectively. The formation and stability of these species at has been proved by the means of quantum chemical calculations and UV−visible absorption spectra.[24b] Figure 1B shows that the UV−visible absorption of C2 and C5, the quinolinium-type structures cations, is very weak.

pH = 3.35−7.40. At these pH values, TPT exists in equilibrium among its enol ((E···H_2O) λ_{abs}^{max} = 374 nm), cation (C1, λ_{abs}^{max} = 381 nm and C4, λ_{abs}^{max} = 382 nm, depending on the pH of the solution), and zwitterion (Z, λ_{abs}^{max} = 409 nm) forms (Scheme 3 for TPT at pH = 7.40). We have previously ascribed (E···H_2O) to E in an open configuration interacting with water molecules through intermolecular H-bonds (iHBs).[30] The growth of Z absorption is clearly shown in the spectrum at pH = 4.35 (Supporting Information, Figure 1S). At physiological conditions (pH = 7.40), the largest population of cationic TPT is in the C4 form. Moreover, at this proton concentration, the ground-state equilibrium involves, in addition to the previous species, the anionic (A) form (Scheme 3). The latter has been

Scheme 2. Schematic Illustration of the Excited-State Protonation of Dicationic TPT (C1) upon Excitation at 371 nm at High (pH ≤ 1.31) Proton Concentrations[a]

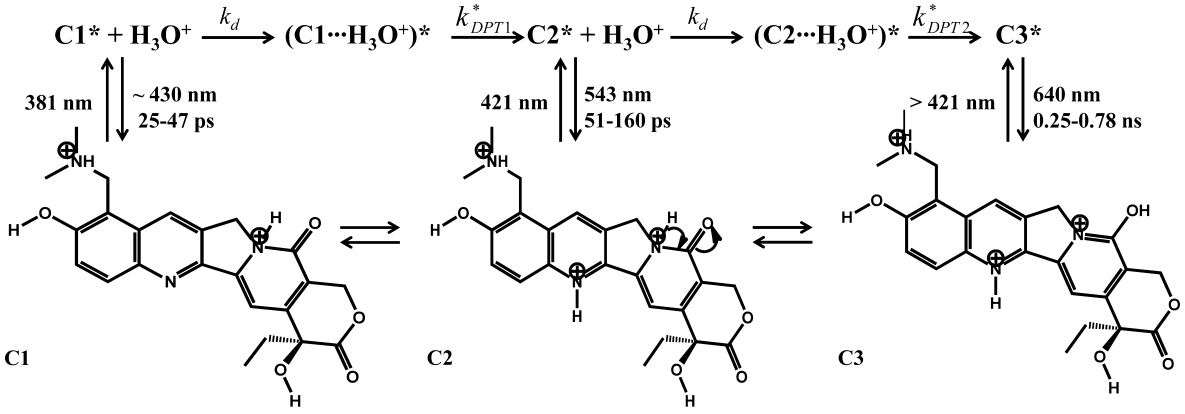

[a] $1/\tau_{C1}$, $1/\tau_{C2}$, and $1/\tau_{C3}$ are the emission rate constants for C1*, C2*, and C3*, respectively. k_d is the rate constant for the diffusion process between the proton and C1* and C2* species. k^*_{DPTl} and k^*_{DPT2} are the direct proton-transfer rate constants for C1* and C2*, respectively. The ground-state equilibrium between C1, C2, and C3 is also shown. The arrows indicate the reaction that leads to the keto−enolic tautomerism between C2 and C3.

dx.doi.org/10.1021/jp303826c | J. Phys. Chem. B 2012, 116, 8182−8190

Scheme 3. Schematic Illustration of the Ground- and Excited-State (upon excitation at 371 nm) Behavior of TPT in Phosphate Buffer Solution at pH = 7.40[a]

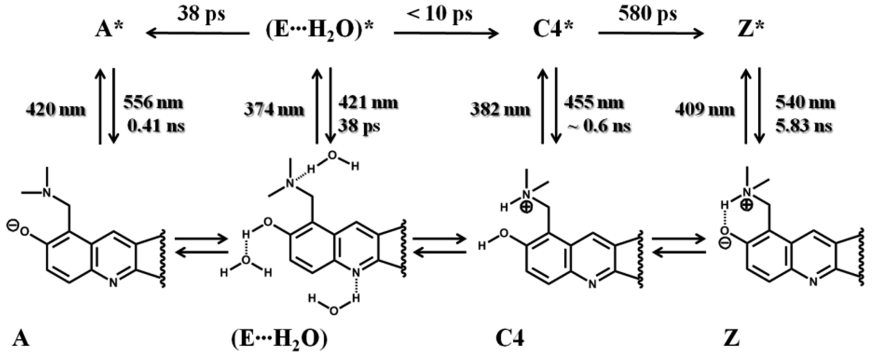

[a]The molecular structures of the involved species ((E···H_2O), C4, Z, and A), with only the quinoline moiety, are shown.

found to prevail in very alkaline conditions (pH = 12.15), showing an absorption spectrum with a maximum at 420 nm.[30]

Emission Spectra. The influence of pH on the emission spectra, which until now has never been reported for this drug, was investigated for the 0.48−7.40 range upon excitation at 371 and 433 nm (Figure 2 and Figures 2S−4S in Supporting Information). We got a rich behavior that varied with the following experimental conditions.

pH = 0.48−1.31. The emission of TPT consists of three fluorescence bands centered at ~430 nm (Stokes shift: $\Delta\bar{\nu}_{ST}$ ~ 3000 cm^{-1}), 543 nm ($\Delta\bar{\nu}_{ST}$ = 7830 cm^{-1}), and 640 nm ($\Delta\bar{\nu}_{ST}$ = 10 622 cm^{-1}) which we assign to C1*, C2* and C3*, respectively (Figure 2A for TPT at pH = 0.78). It is clear from the spectra that the emission intensity ratio at the maxima of C3* and C2* (I_{640}/I_{543}) increases at low pH values (I_{640}/I_{543} = 0.35 and 1.46 at pH = 1.31 and 0.48, respectively), thus indicating a better efficiency of the excited-state formation of C3* at higher proton concentrations. The emission spectrum profile of each species is also reported in the Supporting Information (Figure 3S). The ground-state equilibrium between C1, C2, and C3 is supported from the analysis of the excitation spectra gated at different regions of the emission spectrum (Supporting Information, Figure 4S). In the steady-state emission spectra, we observed a quenching of C1* and C2* fluorescence due to the interaction with protons (Figure 2B), in a similar way to what was found for acidic (1 ≤ pH ≤ 2) aqueous solutions of CPT.[32] We analyzed the data using the Stern−Volmer equation in the first- and second-order in [H^+] for C2* and C1*, respectively (eqs 1 and 2 and the inset of Figure 2B).

$$\frac{F_0}{F} = (1 + K_D[H^+]) \quad (1)$$

$$\frac{F_0}{F} = (1 + K_D[H^+])(1 + K_S[H^+]) \quad (2)$$

F_0 and F are the fluorescence intensities of C1* and C2* in the absence (F_0) and in the presence (F) of an ESPT reaction. K_D and K_S are the dynamic and static quenching constants, respectively. The F_0 values were determined at pH = 1.31 and 0.95 for C1 and C2, respectively. pH = 1.31 is the upper limit at which the dynamics between C1, C2, and C3 still occur. At pH values ≥1.31, both the ground- and excited-state dynamics of TPT change due to the appearance of new tautomeric forms of the drug (vide infra). The characteristic upward curvature of the Stern−Volmer plot indicates a static quenching of C1* emission, accompanying the overall dynamic quenching process (inset of Figure 2B). The experimental data were satisfactory fit using the above equations, giving a square correlation constant $R^2 \geq 0.99$. For the C1* species, we found dynamic and static quenching constants values K_{D1} = 1.54 M^{-1} and K_{S1} = 0.35 M^{-1}, respectively. A higher value of K_{D2} (4.93 M^{-1}) was obtained in the case of C2*.

pH = 1.31−3.35. At this pHs range and exciting at 371 nm, we observed a strong emission centered at 541 nm, whose intensity increases as the proton concentration decreases (Figure 2SA, Supporting Information). We assign this emission to the zwitterionic forms Z and ZN1 (Scheme 2S, Supporting Information). The latter one, showing protonation on the quinoline nitrogen atom, is supposed to predominate at pH = 1.87, which is a value very close to the pK_a* of N1 (1.85, Supporting Information, Table 1S). Similarly to what we found in this work for TPT, a weak emission with maximum at 520 nm has been observed for acidic (pH = 2) aqueous solutions of 10-CPT.[26] It has been assigned to a zwitterionic form of the molecule with protonation on the quinoline moiety. We did not observe emission from C3. This is confirmed also by the spectra obtained upon excitation at 433 nm (Figure 2C), in which the emission from C3* is extremely weak.

pH = 3.35−7.40. At this range, we observed the typical emission from Z* ($\bar{\nu}_{ST(Z^*)}$ ~ 7660 cm^{-1}) as shown in Figure 2A (at pH = 7.40 and exciting at 371 nm) and Figure 2S in the Supporting Information (at pH = 4.35 and upon 371 (A) and 433 (B) nm excitation). In contrast, the fluorescence from the blue-emitting E* (λ_{abs}^{max} of 421 nm, $\Delta\bar{\nu}_{ST(E^*)}$ = 2425 cm^{-1})[30] is very weak. The contribution of A to the total ground-state absorption, being irrelevant in the 3.35−6.24 range, is observed, even in a very little amount, at physiological conditions. This is also supported from the emission lifetimes detected for aqueous solution of TPT at pH = 7.40 upon excitation at 433 nm (vide infra). The contribution of A becomes important only in very alkaline conditions (pH = 12.15).[30]

In summary of this part, due to the multifunctional nature of TPT, there are at least eight possible chemical structures in aqueous solutions: five different cationic structures, whose relative contribution depends on the proton concentration; the neutral and zwitterionic forms, detectable at near neutral pH values; and the anionic form, which contributes in a little amount only at physiological conditions. The absorption as well as the emission spectra of the drug strongly depend on the number, structure, and excited-state reactivity of the TPT structures existing at a given proton concentration.

3.2. Time-Resolved Picosecond Emission Measurements. The picosecond emission decays of TPT in aqueous

dx.doi.org/10.1021/jp303826c | J. Phys. Chem. B 2012, 116, 8182−8190

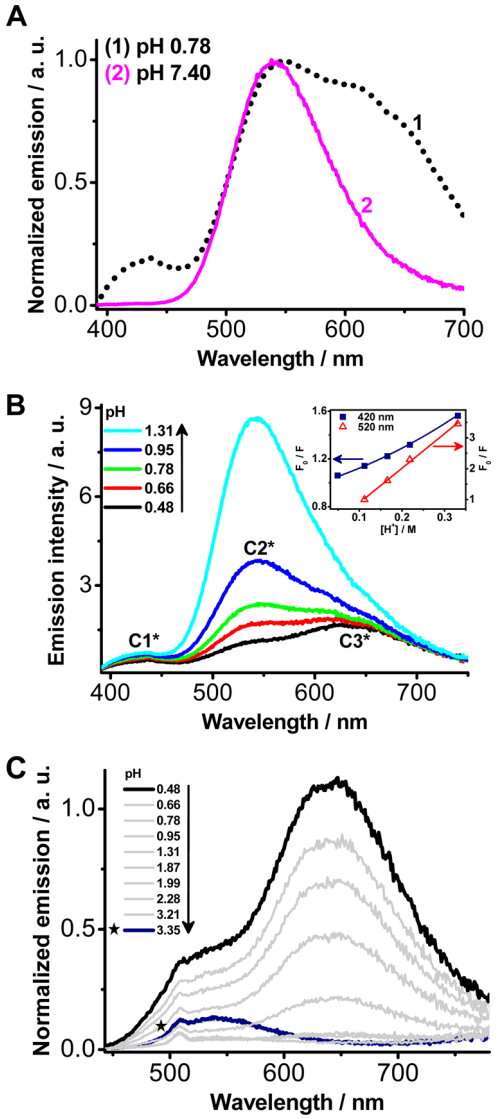

Figure 2. (A) Normalized emission spectra of TPT in acidic water (pH = 0.78) (1) and in phosphate buffer solution (pH = 7.40) (2). The excitation wavelength is at 371 nm. (B) Corrected emission spectra of TPT in aqueous solution in the pH = 0.48−1.31 range. The emission bands of the involved cationic species are marked as C1*, C2*, and C3*. The excitation wavelength is at 371 nm. Inset: fluorescence quenching of C1* (filled squares) and C2* (open triangles) species by the protons. The Stern−Volmer fits for C1* and C2* are shown. (C) Emission spectra of TPT in aqueous solutions at different pH values (0.48 ≤ pH ≤ 3.35). The excitation wavelength is at 433 nm.

solutions of different pH values were carried out exciting at 371 and 433 nm. Table 1 collects the obtained time constants (τ_i) and normalized pre-exponential factors (A_i) in the emission decay of TPT in aqueous solution (λ_{exc} = 371 and 433 nm) at two representative pHs. We used a global analysis ($\chi^2 \leq 1.1$) to derive the fluorescence time constants. The results are here presented and discussed, and they will be focused on very acidic (0.48−1.31) and physiological (7.40) pHs. More details are given in the Supporting Information (Tables 3S−14S).

pH = 0.48−1.31. Upon excitation at 371 nm, the emission decays were fit to an either bi- or triexponential function. Representative dynamics at 371 nm gated at different observation wavelengths are reported for pH = 0.78 (Figure 3B). In addition to that, the effect of pH (0.48−1.31) on the excited-state

Table 1. Values of Fluorescence Time Constants (τ_i) and Normalized (to 100) Pre-Exponential Factors (A_i) of Fitting Decay Functions for TPT in Acidic Water (pH = 0.78) and at Physiological Conditions (phosphate buffer solution at pH = 7.40) at Different Emission Wavelengths (λ_{em})[a]

λ_{exc}/nm	pH	λ_{em}/nm	τ_1/ps (A_1%)	τ_2/ns (A_2%)	τ_3/ns (A_3%)
371	0.78	450	35 (98)	0.10 (2)	
		640	35 (−19)	0.10 (−22)	0.37 (59)
	7.40	450	38 (68)	0.58 (27)	5.73 (5)
		600	38 (−16)	0.58(−5)	5.73 (79)
433	0.78	620		0.10 (3)	0.33 (97)
		660		0.10 (−20)	0.33 (80)
	7.40	460		0.36 (11)	5.83(89)
		620		0.36 (2)	5.83 (98)

[a]The excitation wavelengths are at 371 and 433 nm.

dynamics gated at the blue (450 nm) and red (640 nm) sides are shown, correspondingly, in Figure 5S of the Supporting Information and Figure 4. The obtained lifetimes are τ_1 = 25−47 ps, τ_2 = 0.051−0.16 ns, and τ_3 = 0.25−0.78 ns; see Figure 5A. The first component (τ_1), assigned to the emission decay of C1*, is observed at higher energies (A_1% ≥ 96 at 450 nm). It rises in the 545−640 nm region, with maxima $|A_i|$% values at 580 nm. A second rise in the red region (640 nm) is given from the second component τ_2, corresponding to C2*. It decays in the middle-energies region, having the maximum contribution at 545 nm. The third and last component (τ_3) originates from excited C3 (formed after protonation of C2* on the pyridone group and fast keto−enolic tautomerization) and prevails mostly as a decay at longer wavelengths. The establishment of a S_1 equilibrium between the three structures is supposing to lead to similar decay time constants. However, in our experiments we observed that τ_1, τ_2, and τ_3 have different values. Moreover, under acidic solutions (pH = 0.78) and exciting at 433 nm (Supporting Information, Table 6S), where only the quinolinium-type forms (C2 and C3) absorb, the fluorescence decay showed a biexponential behavior giving lifetimes of 0.10 and 0.33 ns, similar to τ_2 and τ_3, respectively. Thus, the result suggests that, at pH ≤ 1.31, C1* and C2* are not in equilibrium at S_1. A further support to this conclusion is given by the absence of emission from C1* upon excitation at 433 nm at all the investigated pHs (Figure 2C). The absence of an excited-state equilibrium can be also excluded for C2* and C3*, as it was deduced from time-resolved emission spectra (TRES) experiments. Figure 3C displays normalized (at the intensity maxima) TRES of TPT at pH = 0.78 upon excitation at 371 nm. Here, the species C1* (λ_{abs}^{max} = 445 and 500 nm) and C2* (λ_{abs}^{max} = 545 nm) emitting in the 405−580 nm region disappear at the subnanosecond time scale, while that (C3*) fluorescing above 580 nm (λ_{abs}^{max} = 630 nm) has a much longer lifetime. This behavior agrees with the above assignment of three cationic forms of TPT at acid pHs. The lack of the equilibrium at S_1 between C2* and C3* is proved by the complete disappearance of the C2* emission at longer gating times, while the signal from C3* is still detectable. The emission band at 500 nm, which belongs to C1*, is not observed in the steady-state spectrum because it is hidden by the strong fluorescence signal of C2*.

Using the lifetime measurements, we got information on the dynamic quenching observed for the excited cationic species of TPT (eq 3 and Figure 6S in the Supporting Information):

$$\frac{1}{\tau_n} = \frac{1}{\tau_{Cn}} + k_{qn}[H^+] \quad (3)$$

dx.doi.org/10.1021/jp303826c | J. Phys. Chem. B 2012, 116, 8182−8190

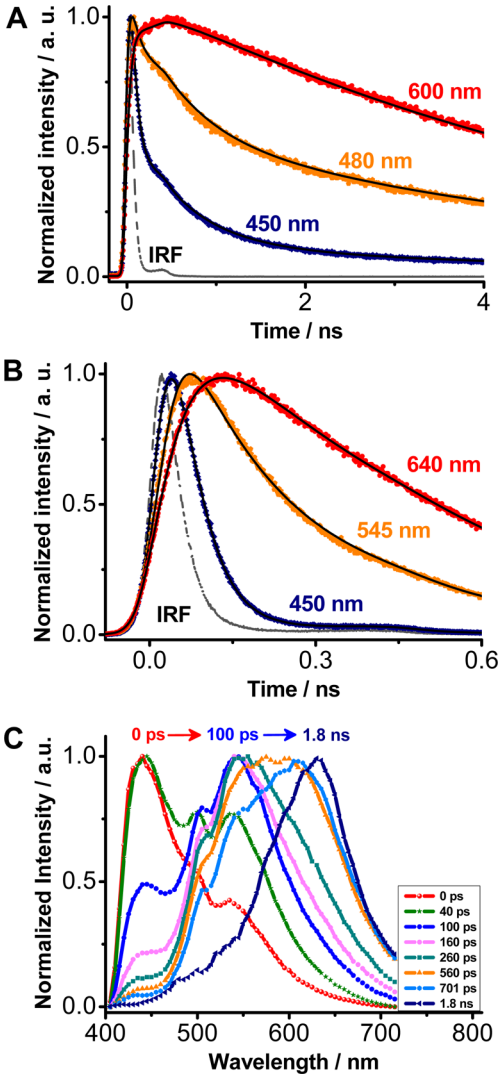

Figure 3. Emission decays of TPT in phosphate buffer (pH = 7.40) (A) and in acidic water (pH = 0.78) (B) solution gated at different wavelengths of observation. The solid lines are the best fit exponential functions, and IRF is the instrumental response function. The excitation wavelength is at 371 nm. (C) Magic-angle time-resolved emission spectra (TRES) of TPT in acidic water solution (pH = 0.78), gated at the indicated delay times after excitation at 371 nm. The inset gives the gating times of the spectra.

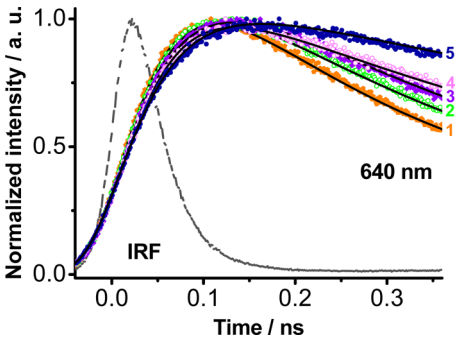

Figure 4. Emission decays of TPT in water gated at 640 nm at pH = 0.48 (1), 0.66 (2), 0.78 (3), 0.95 (4), and 1.31 (5), respectively. The solid lines are the best fit exponential functions, and IRF is the instrumental response function. The excitation was at 371 nm.

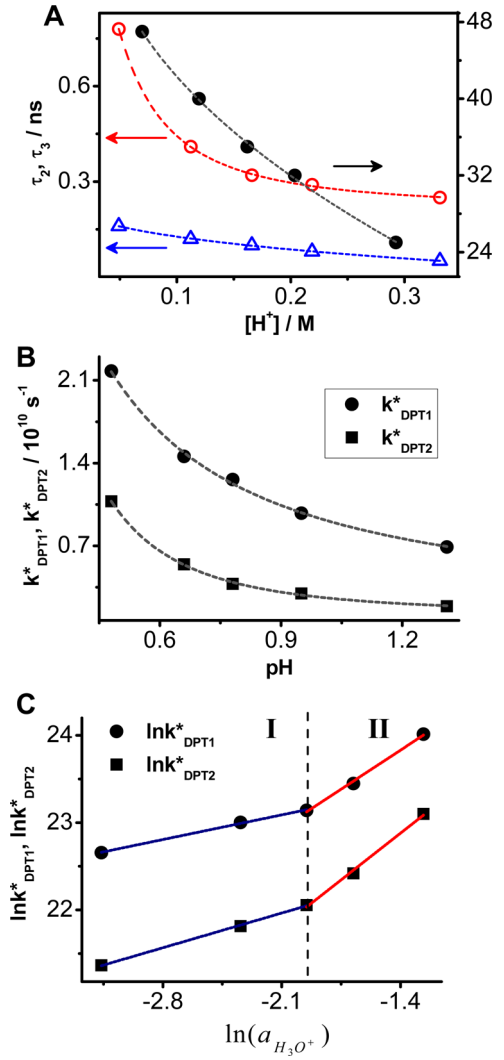

Figure 5. (A) Change of the time constants τ_1 (filled circles), τ_2 (open triangles), and τ_3 (open circles) as a function of the proton concentration in the pH = 0.48−1.31 range. The dashed lines are just to guide the eyes. (B) Change of the direct proton-transfer rate constants k^*_{DPTI} (●) and k^*_{DPT2} (■) as a function of pH in the 0.48−1.31 range. The dashed lines are just to guide the eyes. (C) Linear fit of the logarithm of the direct proton-transfer rate constants k^*_{DPTI} and k^*_{DPT2} as a function of the logarithm of the hydrogen ion activity in the used aqueous solutions.

τ_{Cn} (n = 1−3) is the lifetime of not-quenched Cn* emission extracted from the intercept, τ_n (n = 1−3) is the time constant of the quenched Cn* emission, and k_{qn} (n = 1−3) is the quenching rate constant. In the case of C2*, the lifetime constant for the not-quenched emission was measured at pH = 1.87. At this proton concentration, C2* does not undergoing more excited-state protonation to give C3* (Supporting Information, Table 9S). The experimental rate constants ($1/\tau_n$) were satisfactorily fit to a linear function, giving square correlation constants $R^2 > 0.91$. We obtained k_q values of 1.36 and 1.59×10^{10} M^{-1} s^{-1} for C1* and C2*, respectively, and 7.83×10^9 M^{-1} s^{-1} for C3*. The lifetimes extracted from the intercepts were τ_{C1} = 73 ps, τ_{C2} = 0.29 ns, and τ_{C3} = 0.72 ns. The dynamic quenching constants K_{D1} = 0.99 M^{-1} and K_{D2} = 4.45 M^{-1} relative to C1* and C2*, respectively, well match those (K_{D1} = 1.54 M^{-1}, K_{D2} = 4.93 M^{-1}) obtained from the steady-state measurements.

dx.doi.org/10.1021/jp303826c | J. Phys. Chem. B 2012, 116, 8182−8190

Application of the Debye–Smoluchowski Model. On the basis of these observations, we describe the reaction of C1* and C2* accepting a proton from the acidic water using a four-step diffusive model[32] (Scheme 2). Here, $(C1\cdots H_3O^+)^*$ and $(C2\cdots H_3O^+)^*$ are the H-bonded complexes of C1* and C2*, respectively, with the hydrated proton. The excited-state protonation, leading to C3* as the final photoproduct, is irreversible under these conditions, and it is characterized by the rate constants, k^*_{DPT1} and k^*_{DPT2}, of a direct reaction. k_d is a bimolecular collisional rate constant typical for a system in a diffusion regime, and it is given by the Debye–Smoluchowski equation (eq 4)

$$k_d = \frac{4\pi N_A D R_D}{(1 - \exp(-R_D/a)) \times 1000} \quad (4)$$

where N_A is the Avogadro number; $D = D_{H+} + D_{C1^*,C2^*}$ is the relative photobase–proton diffusion coefficient, which depends on the acid concentration; R_D is the Debye radius; and a is the typical reaction contact radius and ranges from 5.5 to 8 Å.[26,33] We used a = 5.5 Å as in our previous work.[32] The Debye radius $R_D \equiv |z_1 z_2| e^2/k_B T\varepsilon$ ($z_{1,2}$ and e are the ionic and the electronic charge, respectively, ε is the dielectric constant of the medium, k_B is the Boltzmann constant, and T is the temperature) defines the Coloumbic attraction between the proton and the excited cationic forms. Additional details about the determination of the parameters used in the Debye–Smoluchowski model are given in the Supporting Information. The diffusion-controlled reaction rate constant, k_s, for separation of the reaction complex was calculated using eq 5:

$$k_s = \frac{4\pi N_A D R_D}{(\exp(R_D/a) - 1) \times 1000} \quad (5)$$

The relevant parameters for the diffusion step of excited C1 and C2 and protons in the pH = 0.48–1.31 range are summarized in Table 2. At pH = 0.48–1.31, a large number of collisions between the proton and the two species C1* and C2* at N1 and carbonyl D-ring sites, respectively, possess sufficient energy to make the complexes reactive, with the ratio $k_{q1}(k_{q2})/k_d \sim 4$. Increasing the pH to 1.31, the energy barrier for the diffusive step between separated C1* and C2* and H_3O^+ to form the encounter complex increases, as clearly evidenced by the reduction of the ratio (k_{q1}/k_d = 1.03, k_{q2}/k_d = 1.21 at pH = 1.31, Table 3). For a reaction near the diffusion-controlled limit, the diffusion rate constant for the separation of the reaction complex (k_s in Table 2) is lower than the rate constant for the direct proton-transfer reaction and thus can be ignored.

Table 2. Values of the Relevant Parameters for the Diffusion Step of C1*, C2*, and Protons Species in the pH = 0.48–1.31 Range (see the text for clarity)

pH	$D_{H^+} \times 10^5$/ cm^2 s^{-1}	D_{C1^*}, $D_{C2^*} \times 10^6$/cm^2 s^{-1}	$D \times 10^5$/ cm^2 s^{-1}	R_D/Å	$k_d \times 10^{-10}$/ M^{-1} s^{-1}	k_{q1}/k_d (k_{q2}/k_d)	$k_s \times 10^{-10}$/ M^{-1} s^{-1}
0.48	0.29	3.45	0.64	7.90	0.35	3.92 (4.57)	0.033
0.66	0.44	3.48	0.79	7.66	0.44	3.12 (3.63)	0.044
0.78	0.58	3.49	0.93	7.55	0.52	2.62 (3.06)	0.054
0.95	0.86	3.50	1.21	7.44	0.68	2.00 (2.34)	0.073
1.31	1.98	3.51	2.33	7.32	1.32	1.03 (1.21)	0.15

Obviously, the excited-state proton-transfer (ESPT) reaction involves electronically excited species, and thus, one should consider the fluorescence lifetimes of the involved structures: $1/k_{C1} = \tau_{C1}$, $1/k_{C2} = \tau_{C2}$, and $1/k_{C3} = \tau_{C3}$ for C1*, C2*, and C3*, in that order. Emission from $(C1(2)\cdots H_3O^+)^*$ was not observed in our experimental conditions. The kinetic equations that describe the irreversible behavior of the system are given in the Supporting Information. Under these experimental conditions, both the retro protonation of C1* and the second-step protonation of C2* are much faster than deprotonation of the latter, so k^*_{BPTI} (back-reaction) can be neglected in the calculations. The large stabilization of C3* with respect to C2*, which is the main driving force for the second protonation, accounts for the irreversibility of this process. Therefore, k^*_{BPT2} can be also ignored. The values of proton-transfer rate constant (k^*_{DPTI} and k^*_{DPT2}) of direct reaction of TPT in the pH = 0.48–1.31 range are given in Table 3, and their behavior with the pH is depicted in Figure 5B. The data show how the dynamics of excited TPT are strongly influenced by the pH even when the acidity of the surrounding medium varies within a small range. The rate constant values for the direct protonation of C1* and C2* are reduced by a factor of ~1/3 (from 2.18 to 0.69 × 10^{10} s^{-1}) and ~1/6 (from 1.08 to 0.19 × 10^{10} s^{-1}), respectively, as the pH increases up to 1.31. This evidences that diffusion governs the dynamics of the C1*→C2*→C3* reaction in the studied range of pH (0.48–1.31).

Table 3. Values of Direct (k^*_{DPT1} and k^*_{DPT2}) Proton-Transfer Rate Constants and of Other Related Parameters of TPT in HCl Solutions

pH	$a_{H_3O^+}$[a]	k^*_{DPT1} (k^*_{DPT2})/10^{10} s^{-1}	τ_{DPT1} (τ_{DPT2})/ps
0.48	0.2824	2.18 (1.08)	46 (93)
0.66	0.1868	1.46 (0.54)	69 (183)
0.78	0.1418	1.26 (0.38)	79 (264)
0.95	0.0961	0.98 (0.30)	102 (336)
1.31	0.0423	0.69 (0.19)	145 (526)

[a]From ref 34.

The correlation between k^*_{DPTI} and k^*_{DPT2} with the activity of H_3O^+ was analyzed according to the empirical expression used also for CPT[32]

$$\ln k^*_{DPT} = \ln(k^*_{DPT})_0 + n \ln(a_{H_3O^+}) \quad (6)$$

where $a_{H_3O^+}$ is the activity of H_3O^+ and n reflects the number of protons involved in the retro-proton-transfer step. k^*_{DPTI} is the rate constant of protonation when $a_{H_3O^+}$ = 1, and thus, the intrinsic proton-transfer rate constant in the "static" reaction limit. Figure 5C shows the obtained result using the above equation to fit the experimental data. As for CPT, we can clearly distinguish two regions (I and II): in the first one (I, pH = 1.31–0.78) we obtained $n \sim 1$. $(k^*_{DPT})_0$ and $(\tau_{DPT})_0$ were known from the slope and the intercept, respectively $(k^*_{DPT1(2)})_0$ = 2.48 (1.14) × 10^{10} s^{-1}, $(\tau_{DPT1(2)})_0$ = 40 (88) ps. For the more acidic region (II, pH = 0.78–0.48), the data were best fit using a linear function with higher values for the slope and intercept: $n = 2 \pm 0.2$ and $(k^*_{DPT1(2)})_0$ = 1.34 (0.73) × 10^{11} s^{-1}, $(\tau_{DPT1(2)})_0$ = 7 (14) ps, respectively. Therefore, we associate $n \sim 1$ to the number of hydrogen ions (either Eigen or Zundel)[32] that are in contact with the TPT molecule in the first region of pH (1.31–0.78). The higher value of n (~2), found in very acidic conditions (pH = 0.78–0.48), reflects the probability of finding protons in the outer solvation shell.

pH = 7.40. Figure 3A shows the emission decays of TPT in phosphate buffer at pH = 7.40 upon excitation at 371 nm (where

dx.doi.org/10.1021/jp303826c | J. Phys. Chem. B 2012, 116, 8182–8190

mainly E and C4 forms absorb, while Z and A absorb in a less amount) and gated at different emission wavelengths. Here, the experimental decays were fit to three-exponential functions at all the observation wavelengths (Table 1 and Supporting Information, Table 13S). Two short decaying components (τ_1 = 38 ps and τ_2 = 0.58 ns) are detected in the 450−520 nm region. The first component prevails at 450 nm (A_1% = 68), while the second one shows its maximum contribution at 480 nm. Both τ_1 and τ_2 rise at lower energies of the spectral emission, with absolute contributions ($|A_i|$%) being maxima at 650 and 560 nm for τ_1 and τ_2, respectively. A 5.73 ns component, τ_3, is decaying at all the wavelength of observation, with maxima A_3% values at 540 nm. On the basis of our previous finding, we state that the excited-state reactions of TPT observed at physiological conditions are similar to those occurring at near neutral pH (6.24).[30] Upon the 371 nm excitation, E* undergoes both fast (38 ps) and very fast (less than 10 ps) excited-state proton-transfer reaction with the solvent molecules giving the A* (deprotonation of the 10-OH group) and the C4* (protonation the 9-dimethylaminomethylene group) forms, respectively. A slow deprotonation (580 ps) of C4* within its lifetime (~0.6 ns)[30] gives Z* (τ_{Z^*} = 5.73 ns) as the final photoproduct. The generated A relaxes to S_0 with a lifetime of 0.41 ns (determined at pH = 12.15),[30] which we did not observed in the emission decay because it should be masked by the presence of the rise, in the same region, of the 580 ns-component. A very fast channel for the Z* formation from E structures less interacting with the solvent, and thus, more reactive, could also occur. The observation of different deprotonation rates for $(E\cdots H_2O)^*$ (38 ps) and C4* (580 ps) forms has been explained in terms of different H-bond interactions between the excited solute and the water molecules. The higher excited-state acidity (in terms of pK_a^*) of the 10-OH group in $(E\cdots H_2O)^*$ with repect to that in C4* makes the proton-transfer event faster for $(E\cdots H_2O)^*$ than for C4*. Like in pure water at pH = 6.24, we did not find any evidence for geminate recombination leading to the back-ESPT. However, the presence of the phosphate anion in the buffer solution has the effect to reduce the time constants of deprotonation (from 42 to 38 ps and from 680 to 580 ps for $(E\cdots H_2O)^*$ and C4* in pure water and in buffer solution, respectively). Previously, it was shown that small amounts of base in low concentrations in the aqueous solutions can affect the geminate recombination by acting as scavengers for the ejected protons, without directly influencing the rate of the proton-transfer reaction.[35] However, in our case, a small effect on the rate of proton-transfer reaction is observed. Excitation at 433 nm, where Z is the main absorbing species, provides two lifetimes of 0.49 and 5.83 ns, the latter having a very large contribution (89−99%) at all the wavelengths of observation (Supporting Information, Table 14S). This confirms the previous assignation made for Z*. The shorter time should correspond to the average time between C4* (τ_{C4^*} ~ 0.6 ns) and A* (τ_{A^*} = 0.41 ns).

Summarizing, in aqueous solutions in the pH = 0.48−7.40 range, the S_1 dynamics of TPT are characterized by bi- or three-exponential fluorescence decays, depending on the species involved at a given proton concentration and excitation wavelength. In phosphate buffer solution (pH = 7.40), a ground-state equilibrium is established between E, C, and, to a small extent, Z and A forms. The nature of the solute as well as the H-bonds network between the molecule with the water molecules at both the ground- and the excited-states plays a key role in the proton-transfer reaction rates. The dynamics of the cationic species involved at more acidic conditions (pH ≤ 3.35) strongly depends on the proton concentration. Diffusion governs the protonation at pH = 0.48−1.31.

4. CONCLUSIONS

The results described and discussed in this work reveal, for the first time, the rich structural dynamics of the anticancer drug TPT in aqueous solutions of different pHs (0.48−7.40). In all the studied solvents, the drug shows multiple emission due to the establishment of efficient proton-transfer reactions between the excited structures of the drug with the water molecules. In aqueous solution at physiological conditions (pH = 7.40), a ground-state equilibrium is established between E, C, and Z forms. The nature of the solute as well as the H-bonds network between the molecule with the water molecules at both the ground and excited states affect the proton-transfer reaction rates. In the pH = 0.48−1.31 region, the proton motion from the acidic solution to the C forms of TPT is governed by the diffusion. Under these conditions, we observed both dynamic and static quenching by protons. The ESPT time constants largely depend on the proton concentration. The number of protons involved in the proton-transfer changes from ~2, for the more acidic region (pH = 0.48−0.78), to ~1, for the less acidic one (pH = 0.78−1.31). The reactions of intermolecular H bonds explored here are reminiscent of those of many chemical and biological/natural systems. We believe that these results provide insights on the role of the H-bonding surroundings on the conformational, structural, and dynamical properties of aqueous solutions of TPT.

■ ASSOCIATED CONTENT

Supporting Information

Absorption, excitation, emission spectra, and time-resolved picoseconds measurements (upon excitation at 371 and 433 nm) of TPT in the aqueous solutions used in this work, the dynamic quenching of TPT by the protons in the pH = 0.48−1.31 range, details on the application of the Debye−Smoluchowski model, and the kinetic equations extracted for the 0.48 ≤ pH ≤ 1.31 regime. This material is available free of charge via the Internet at http://pubs.acs.org.

■ AUTHOR INFORMATION

Corresponding Author

*E-mail: Abderrazzak.Douhal@uclm.es. Fax: +34-925-268840. Phone: +34-925-265717.

Notes

The authors declare no competing financial interest.

■ ACKNOWLEDGMENTS

This work was supported by the MICINN through project MAT2008-01609. M.R.d.N. and Y.L.W. thank CYCLON Network (MRTN-CT-2008-Project 237962) for the Marie Curie fellowship.

■ REFERENCES

(1) Bailly, C. *Crit. Rev. Oncol. Hematol.* **2003**, *45*, 91−108.
(2) Nagourney, R. A.; Sommers, B. L.; Harper, S. M.; Radecki, S.; Evans, S. S. *Br. J. Cancer* **2003**, *89*, 1789−95.
(3) Garcia-Carbonero, R.; Supko, J. G. *Clin. Cancer Res.* **2002**, *8*, 641−661.
(4) Wall, M. E.; Wani, M. C.; Cook, C. E.; Palmer, K. H.; Mcphail, A. T.; Sim, G. A. *J. Am. Chem. Soc.* **1966**, *88*, 3888−3890.
(5) D'Arpa, P.; Liu, L. F. *Biochim. Biophys. Acta* **1989**, *989*, 163−177.
(6) Pommier, Y. *Nat. Rev. Cancer* **2006**, *6*, 789−802.

(7) Pommier, Y.; Pourquier, P.; Fan, Y.; Strumberg, D. *Biochim. Biophys. Acta (BBA): Gene Struct. Expression* **1998**, *1400*, 83−106.
(8) Siu, F. M.; Che, C. M. *J. Am. Chem. Soc.* **2008**, *130* (52), 17928−17937.
(9) Pommier, Y.; Pourquier, P.; Urasaki, Y.; Wu, J.; Laco, G. S. *Drug Resist. Updates* **1999**, *2*, 307−318.
(10) Sehouli, J.; Oskay-Oezcelik, G. *Curr. Med. Res. Opin.* **2009**, *25*, 639−651.
(11) Nicum, S. J.; O'Brien, M. E. R. *Expert Rev. Anticancer Ther.* **2007**, *7*, 795−801.
(12) Idris, T.; Winter, R.; Lang, U.; Petru, E. *Anticancer Res.* **2009**, *29*, 1761−1762.
(13) Itoh, M.; Adachi, T.; Tokumura, K. *J. Am. Chem. Soc.* **1984**, *106*, 850−855.
(14) Poizat, O.; Bardez, E.; Buntinx, G.; Alain, V. *J. Phys. Chem. A* **2004**, *108*, 1873−1880.
(15) Kwon, O. H.; Kim, T. G.; Lee, Y. S.; Jang, D. J. *J. Phys. Chem. B* **2006**, *110*, 11997−12004.
(16) Angulo, G.; Organero, J. A.; Carranza, M. A.; Douhal, A. *J. Phys. Chem. B* **2006**, *110*, 24231−24237.
(17) Fassberg, J.; Stella, V. J. *J. Pharm. Sci.* **1992**, *81*, 676−684.
(18) Dey, J.; Warner, I. M. *J. Photochem. Photobiol., A* **1998**, *116*, 27−37.
(19) Nabiev, I.; Fleury, F.; Kudelina, I.; Pommier, Y.; Charton, F.; Riou, J. -F.; Alix, A. J. P.; Manfait, M. *Biochem. Pharmacol.* **1998**, *55*, 1163−1174.
(20) Chauvier, D.; Chourpa, I.; Maizieres, M.; Riou, J. -F.; Dauchez, M.; Alix, A. J. P.; Manfait, M. *J. Mol. Struct.* **2003**, *651*−*653*, 55−65.
(21) Strel'tsov, S. A.; Grokhovskii, S. L.; Kudelina, I. A.; Oleinikov, V. A.; Zhuze, A. L. *Mol. Biol.* **2001**, *35*, 365−373 and references therein.
(22) Gryczynski, I.; Gryczynski, Z.; Lakowicz, J. R.; Yang, D.; Burke, T. G. *Photochem. Photobiol.* **1999**, *69* (4), 421−428.
(23) Posokhov, Y.; Biner, H.; Icüli, S. *J. Photochem. Photobiol., A* **2003**, *158*, 13−20.
(24) (a) Sanna, N.; Chillemi, G.; Grandi, A.; Castelli, S.; Desideri, A.; Barone, V. *J. Am. Chem. Soc.* **2005**, *127*, 15429−15436. (b) Ivanova, B.; Spiteller, M. *Biopolymers* **2012**, *97*, 134−144.
(25) Das, K.; Smirnov, A. V.; Wen, J.; Miskovsky, P.; Petrich, J. W. *Photochem. Photobiol.* **1999**, *69*, 633−645.
(26) Solntsev, K. M.; Sullivan, E. N.; Tolbert, L. M.; Ashkenazi, S.; Leiderman, P.; Huppert, D. *J. Am. Chem. Soc.* **2004**, *126*, 12701−12708.
(27) El-Kemary, M.; Gil, M.; Douhal, A. *J. Med. Chem.* **2007**, *50*, 2896−2902.
(28) Gil, M.; Douhal, A. *J. Phys. Chem. A* **2008**, *112*, 8231−8237.
(29) Cohen, B.; Organero, J. A.; Santos, L.; Padial, L. R.; Douhal, A. *J. Phys. Chem. B* **2010**, *114*, 14787−14795.
(30) di Nunzio, M. R.; Wang, Y.; Douhal, A. *J. Phys. Chem. B* **2012**, *116*, 7522.
(31) Organero, J. A.; Tormo, L.; Douhal, A. *Chem. Phys. Lett.* **2002**, *263*, 409−414.
(32) di Nunzio, M. R.; Cohen, B.; Douhal, A. *J. Phys. Chem. A* **2011**, *115*, 5094−5104 and references therein.
(33) Rini, M.; Magnes, B. Z.; Pines, E.; Nibbering, E. T. J. *Science* **2003**, *301*, 349−352.
(34) Macinnes, D. A. *J. Am. Chem. Soc.* **1919**, *41*, 1086−1092.
(35) Goldberg, S. Y.; Pines, E.; Huppert, D. *Chem. Phys. Lett.* **1992**, *192*, 77−81.